SCIENCE CHINA
Physics, Mechanics & Astronomy

• Article •

October 2015 Vol. 58 No. 10: 106801
doi: 10.1007/s11433-015-5703-6

Two-dimensional silicon-carbon hybrids with a honeycomb lattice: New family for two-dimensional photovoltaic materials[†]

ZHANG Jin[1], REN Jun[2*], FU HuiXia[1], DING ZiJing[1], LI Hui[1*] & MENG Sheng[1,3*]

[1] *Beijing National Laboratory for Condensed Matter Physics, Institute of Physics, Chinese Academy of Sciences, Beijing 100190, China;*
[2] *Department of Physics, Tsinghua University, Beijing 100084, China;*
[3] *Collaborative Innovation Center of Quantum Matter, Beijing 100190, China*

Received April 15, 2015; accepted May 20, 2015

We predict a series of new two-dimensional (2D) inorganic materials made of silicon and carbon elements (2D $\mathrm{Si}_x\mathrm{C}_{1-x}$) based on density functional theory. Our calculations on optimized structure, phonon dispersion, and finite temperature molecular dynamics confirm the stability of 2D $\mathrm{Si}_x\mathrm{C}_{1-x}$ sheets in a two-dimensional, graphene-like, honeycomb lattice. The electronic band gaps vary from zero to 2.5 eV as the ratio x changes in 2D $\mathrm{Si}_x\mathrm{C}_{1-x}$ changes, suggesting a versatile electronic structure in these sheets. Interestingly, among these structures $\mathrm{Si}_{0.25}\mathrm{C}_{0.75}$ and $\mathrm{Si}_{0.75}\mathrm{C}_{0.25}$ with graphene-like superlattices are semimetals with zero band gap as their π and π^* bands cross linearly at the Fermi level. Atomic structural searches based on particle-swarm optimization show that the ordered 2D $\mathrm{Si}_x\mathrm{C}_{1-x}$ structures are energetically favorable. Optical absorption calculations demonstrate that the 2D silicon-carbon hybrid materials have strong photoabsorption in visible light region, which hold promising potential in photovoltaic applications. Such unique electronic and optical properties in 2D $\mathrm{Si}_x\mathrm{C}_{1-x}$ have profound implications in nanoelectronic and photovoltaic device applications.

2D Si-C hybrids, electronic structure, photovoltaic materials, first-principles calculations

PACS number(s): 61.48.-w, 73.22.-f, 71.15.Mb

Citation: Zhang J, Ren J, Fu H X, et al. Two-dimensional silicon-carbon hybrids with a honeycomb lattice: new family for two-dimensional photovoltaic materials. Sci China-Phys Mech Astron, 2015, 58: 106801, doi: 10.1007/s11433-015-5703-6

1 Introduction

Graphene [1,2], an isolated layer of graphite, has attracted great attentions since it was firstly produced in 2004, due to its intriguing structure and electronic properties, such as one-atom thickness, very strong mechanic property, extremely high electron mobility, high thermal conductivity, and room temperature quantum Hall effect [3,4]. Recently, silicene, a monolayer of silicon atoms arranged in graphene-like honeycomb lattices, has been discovered in both theoretical calculations and experiments [5–11]. Many novel quantum properties in graphene can been also found in silicene, for example, both graphene and silicene have linear dispersion Dirac cones around the Fermi level [1,12]. Besides, silicene also exhibits many other extraordinary quantum properties, for instance, it could support experimentally accessible quantum spin Hall effect [6]. Two-dimensional SiC hybrid material [13,14], however, has been predicted to be semiconductors with a very large band gap of 2.5 eV, indicating that the hybridization of silicon and carbon atoms in two dimensions can produce a variety of electronic properties.

Graphene could be considered as a prototypical material for a myriad of two-dimensional (2D) nanostructures. In recent years, 2D materials similar to graphene have been

---

*Corresponding author (REN Jun, email: junren@mail.tsinghua.edu.cn; LI Hui, email: huili8@iphy.ac.cn; MENG Sheng, email: smeng@iphy.ac.cn)
†Recommended by JIN KuiJuan (Associate Editor)

intensively investigated [15–17]. For instance, monolayered transition metal dichalcogenides (TMDs) [18–20] can be obtained from either exfoliation of bulk materials or bottom-up synthesis. Many 2D TMDs are direct-gap semiconductors whose energy gaps and carrier types depend on their composition, atomic structure and dimensionality. Both graphene and monolayer TMDs are promising materials for next-generation 2D optoelectronic devices. Thanks to their semiconducting character, TMD monolayers can serve as sunlight absorbers and enable ultrathin photovoltaic (PV) devices [18–20]. They hold a great potential for solar cell and other optoelectronic applications [21–23].

In this article, we perform first-principles calculations based on density functional theory (DFT) to systematically study a new family of 2D materials: 2D silicon-carbon hybrid compounds. The structures, thermal stabilities, electronic structures as well as optical properties of the 2D silicon-carbon hybrids with various Si/C ratios (ranging from 1:7 to 7:1) have been investigated. We find silicon-carbon hybrids with different ratios can exhibit distinct electronic and optical properties. For instance, 2D $Si_{0.25}C_{0.75}$ and $Si_{0.75}C_{0.25}$ sheets with graphene-like superlattices have zero-gap Dirac cones similar to graphene and silicene, but all other Si_xC_{1-x} structures have significant band gaps ranging from 0.2 eV to 2.5 eV. The phonon dispersion calculations and first-principles molecular dynamics (FPMD) simulations show that these 2D silicon-carbon hybrids are thermodynamically stable. This study suggests that the band structures of 2D Si_xC_{1-x} are tunable and the transitions from semiconductors to zero-gap semimetals can be observed by varying the Si/C ratio and atomic structures. The 2D silicon-carbon hybrid materials have strong photoabsorption in visible light region, which hold promising potential in photovoltaic applications. Therefore, this work provides important guidance for the design of the 2D carbon and silicon based nano-devices.

2 Computational methods

The calculations on 2D Si_xC_{1-x} are performed within the framework of density functional theory using the vienna ab-initio simulation package (VASP) [24,25]. The projector-augmented wave (PAW) [26] method for core region and the generalized gradient approximation with the Perdew, Burke, and Ernzerhof (PBE) [27] functional are employed, taking a plane-wave basis set with an energy cutoff of 500 eV. For geometric optimization, both lattice constants and atomic positions are relaxed until the forces on atoms are less than 10^{-2} eV/Å and the total energy change is less than 10^{-4} eV. The Brillouin zone is sampled by a set of 25×25×1 k-points. The thickness of vacuum layer is set to be 15 Å so that artificial interlayer interactions are avoided.

The particle-swarm optimization (PSO) multidimensional method implemented in the CALYPSO code [28] is employed to search for low-energy structures. The PSO simulations set the population size at 30, and the number of generations is maintained at 30. The structure relaxation during the PSO simulation is performed in VASP. The low-energy structures predicted by PSO are further reoptimized using VASP.

During geometrical optimization in DFT calculations, the structures may be local minima instead of global minimum. Molecular dynamics (MD) simulations are thus performed to assess the thermal stability of local structures as implemented in the VASP code. At each temperature, MD simulations in constant volume and temperature ensemble last for 5 ps using a time step of 2 fs. To confirm the stability of the 2D structures, phonon dispersions are also performed using the force constant method as implemented in the Phonopy [29,30] program.

3 Results and discussion

We consider the 2D Si-C hybrids with nine different Si concentrations. First we produce a 2×2 unit cell of graphene, in which carbon atoms are gradually substituted by silicon atoms to obtain different Si/C ratios. For graphene, $Si_{0.125}C_{0.875}$, $Si_{0.875}C_{0.125}$, and silicene, only one configuration can be obtained in a 2×2 honeycomb unit cell, but for $Si_{0.25}C_{0.75}$, $Si_{0.375}C_{0.625}$, $Si_{0.5}C_{0.5}$, $Si_{0.625}C_{0.375}$, $Si_{0.75}C_{0.25}$, there are several nonequivalent configurations at each ratio. After relaxing all of these configurations for different Si_xC_{1-x}, the cohesive energies are compared to obtain the most stable configuration. Other configurations with low cohesive energies are neglected in the following discussion.

Figure 1 presents the optimized lattice parameter and atomic structure of 2D Si_xC_{1-x} with different Si fractions. Graphene with a stable planar honeycomb lattice is shown in Figure 1(a). The silicene structure in Figure 1(i), on the other hand, has a low-buckled structure with a buckling height of 0.45 Å, in excellent agreement with previous studies [5,13]. Si-C hybrids including $Si_{0.125}C_{0.875}$, $Si_{0.375}C_{0.625}$, $Si_{0.625}C_{0.375}$ and $Si_{0.875}C_{0.125}$ all have a buckled structure comprising of slightly distorted hexagons. Figure 1(b) shows the atomic geometry of $Si_{0.125}C_{0.875}$, which has a lattice constant of 5.30 Å. The $Si_{0.5}C_{0.5}$ in Figure 1(e), however, is found to be completely planar, which prefers sp^2 hybridization between Si and C atoms.

Figure 1(c) presents the atomic structure of $Si_{0.25}C_{0.75}$ sheet obtained from structural optimization. The length of Bravais vectors of the hexagonal lattice is 5.63 Å. The C—C bond length is 1.44 Å, a little larger than that in graphene (about 1.42 Å), while the Si—C bond length is 1.80 Å, smaller than the Si—C bond length in bulk SiC (1.89 Å). The planar nature of 2D $Si_{0.25}C_{0.75}$ sheet is further tested by displacing Si and C atoms out-of-plane arbitrarily from their equilibrium positions. After optimization, all atoms return to the same plane. We conclude that $Si_{0.25}C_{0.75}$ is a one-atom

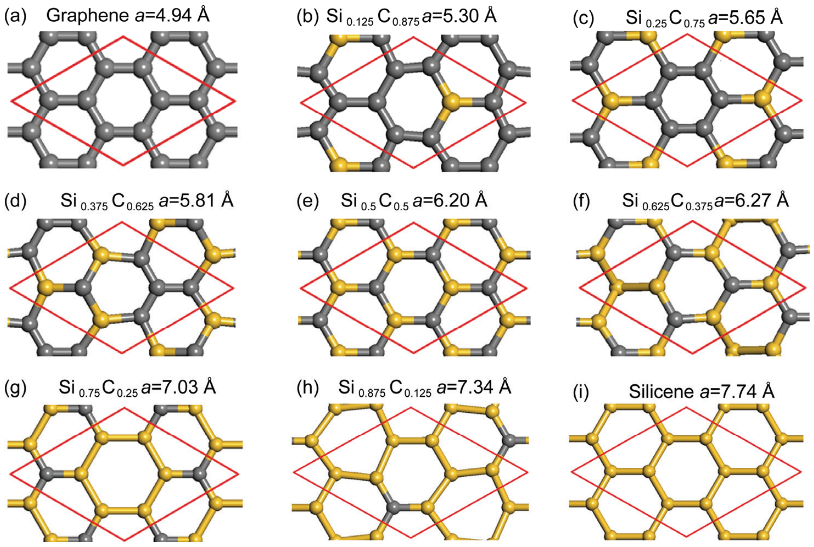

Figure 1 (Color online) Top view of geometric structures with 2D honeycomb configuration for different Si fraction x: (a) graphene; (b) $Si_{0.125}C_{0.875}$; (c) $Si_{0.25}C_{0.75}$ (G-2); (d) $Si_{0.375}C_{0.625}$; (e) $Si_{0.5}C_{0.5}$; (f) $Si_{0.625}C_{0.375}$; (g) $Si_{0.75}C_{0.25}$ (S-2); (h) $Si_{0.875}C_{0.125}$; and (i) silicene. The primitive unit cells are delineated in red rhombuses and lattice constants are also given in each panel. Gray balls and yellow balls denote carbon atoms and silicon atoms, respectively.

thick carbon-silicon sheet arranged in a honeycomb lattice resembling the graphene structure more than the low buckling silicene structure.

The $Si_{0.75}C_{0.25}$ structure shown in Figure 1(g) also consists of two-dimensional honeycomb structure with a larger lattice constant (7.03 Å) compared to that for $Si_{0.25}C_{0.75}$ (5.63 Å), due to larger Si concentration. Different from silicene with a low-buckled structure, all of the atoms of $Si_{0.75}C_{0.25}$ are also positioned in the same plane, namely, it is perfectly planar. Akin to graphene, all the bond angles in $Si_{0.25}C_{0.75}$ and $Si_{0.75}C_{0.25}$ are 120° without any distortion, suggesting sp^2 hybridization is preferred in these structures. Here, $Si_{0.25}C_{0.75}$ and $Si_{0.75}C_{0.25}$ can be viewed as silicon doped graphene with honeycomb superstructures.

Figure 2(a) presents the cohesive energies (in eV/atom) of 2D Si_xC_{1-x} with a honeycomb lattice as a function of the Si fraction. The cohesive energy is defined as:

$$E_{\mathrm{coh}} = E_{\mathrm{Si}_x\mathrm{C}_{1-x}} - xE_{\mathrm{Si}} - (1-x)E_{\mathrm{C}},$$

where E_{Si}, E_{C}, $E_{\mathrm{Si}_x\mathrm{C}_{1-x}}$ are the total energy of an isolated silicon atom, an isolated carbon atom, and the 2D Si_xC_{1-x} compound (per atom), respectively. Graphene has the largest cohesive energy (in absolute values), suggesting strong structural stability compared with other Si_xC_{1-x} sheets. For each 2D Si_xC_{1-x} composition the calculated cohesive energy of low-energy structures are shown as square symbols in Figure 2(a). We find that the relative energy increases almost linearly as the Si concentration in Si_xC_{1-x} increases, implying all these structures can be maintained stable with minimal formation energy relative to graphene and silicene. We also observe that with the increase of the Si fraction x, the lattice constant also linearly increases from the value of 4.92 Å for pure graphene to 7.75 Å for pure silicene (Figure 2(b)). Lattice constants for other Si-C structures are located between the two limits.

For $Si_{0.25}C_{0.75}$, different configurations are predicted from the PSO structural searches. The obtained atomic structure arrangements are shown in Figure 3. The low-energy structures are labeled as G-1, G-2, G-3… in the order of increasing total energy. PSO calculations have confirmed the existence of $Si_{0.25}C_{0.75}$ in a graphene-like honeycomb superlattice mentioned above (G-2), and a new 2D $Si_{0.25}C_{0.75}$ structure (G-1) is also found. The two structures have almost the same energy with the cohesive energy difference as small as 4 meV, indicating both structures are stable. We note that G-1, G-2, and G-4 all have a perfect planar geometry with honeycomb lattices and can thus be viewed as silicon doped graphene, while G-3 and G-5 have a different topological ring structure with distorted four-, five- and seven-membered rings. Interestingly, G-4 and G-5 are stripe-like composed of alternative silicon chains and carbon chains.

The predicted stable 2D $Si_{0.75}C_{0.25}$ structures are shown in Figure 4. The $Si_{0.75}C_{0.25}$ in a perfect honeycomb superlattice (S-2) is one of low-energy structures. For the most stable $Si_{0.75}C_{0.25}$ structure (S-1), the unit cell is in a rectangular shape with lattice constants of 6.05 and 6.93 Å, respectively. All the atoms in the sheet bond to three neighboring atoms in the same plane. The $Si_{0.75}C_{0.25}$ (S-2) has a cohesive energy only 17 meV smaller than that of $Si_{0.75}C_{0.25}$ (S-1). The structure of S-3 is quite similar to that of S-1, only with positions of some silicon and carbon atoms altered. S-4 and S-5 consist of different topological ring structures, resulting in a higher total energy shown in Figure 2(a).

Our PSO calculations show that: (i) The $Si_{0.25}C_{0.75}$ (G-2) and $Si_{0.75}C_{0.25}$ (S-2) sheets with superstructures are energetically favorable, which are among the low-energy structures, (ii) the number of Si—C bonds is found to be maximized

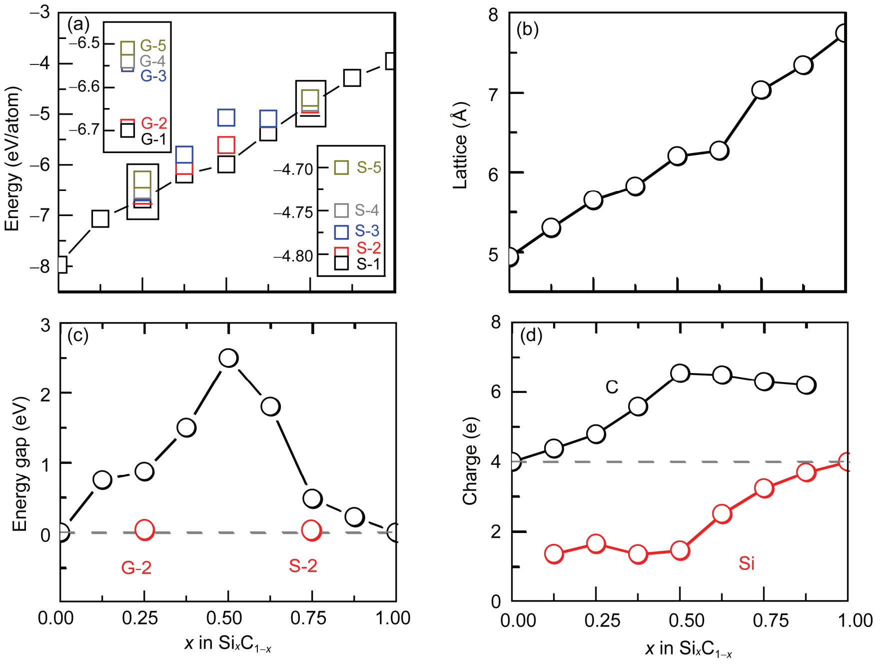

Figure 2 (Color online) (a) The cohesive energy (eV/atom) for Si_xC_{1-x} at different Si fraction x. Inset: zooming in the energy range for $Si_{0.25}C_{0.75}$ and $Si_{0.75}C_{0.25}$ structures; (b) the lattice constant (Å); (c) energy band gaps (eV) at different Si composition (the band gaps for G-2 and S-2 are also given); and (d) bader charges on each Si and C atom in Si_xC_{1-x} structures with different Si fraction x.

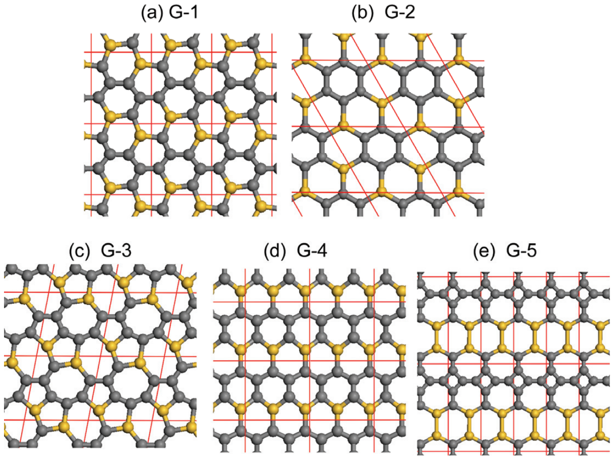

Figure 3 (Color online) Top view of geometric structures of $Si_{0.25}C_{0.75}$ from structural search. Structures from G-1 to G-5 are listed according to their relative energy per atom.

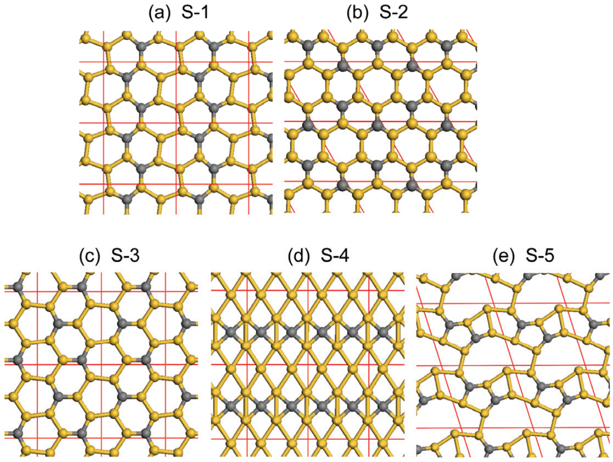

Figure 4 (Color online) Top view of geometric structures of $Si_{0.75}C_{0.25}$ from structural search. Structures from S-1 to S-5 are listed according to their relative energy per atom.

in these configurations. The structures will be seriously distorted if there are direct Si—Si bonds present in $Si_{0.25}C_{0.75}$ (or C—C bonds in $Si_{0.75}C_{0.25}$) because of the bond length imbalance with the neighboring bonds in such structures.

Electronic band structures for these 2D hybrids Si_xC_{1-x} are also calculated and are shown in Figure 5. Our results confirm that graphene is a semimetal with Dirac cones at *K* point, which is in agreement with previous works [5,6]. Silicon-carbon hybrid compounds can open considerable electronic gaps. For instance, the $Si_{0.125}C_{0.875}$ has a direct band gap of 0.80 eV with the valence band maximum (VBM) and the conduction band maximum (CBM) located at *K* point shown in Figure 5(b). As the silicon concentration x increases, the band gap grows larger, which is 0.84 eV for $Si_{0.25}C_{0.75}$ (G-1) and 1.51 eV for $Si_{0.375}C_{0.625}$. Interestingly, we find a direct-to-indirect band gap transition at x=0.375. The $Si_{0.375}C_{0.625}$ structure has the VBM located at *K* point but the CBM located at Γ point. For $Si_{0.5}C_{0.5}$, the band gap reaches the maximum (2.5 eV). Among Si-rich hybrids, $Si_{0.75}C_{0.25}$ (S-1) is a semiconductor with a direct gap of 0.70 eV, and $Si_{0.625}C_{0.375}$ and $Si_{0.875}C_{0.125}$ are indirect semiconductors with band gaps of 1.80 and 0.22 eV, respectively.

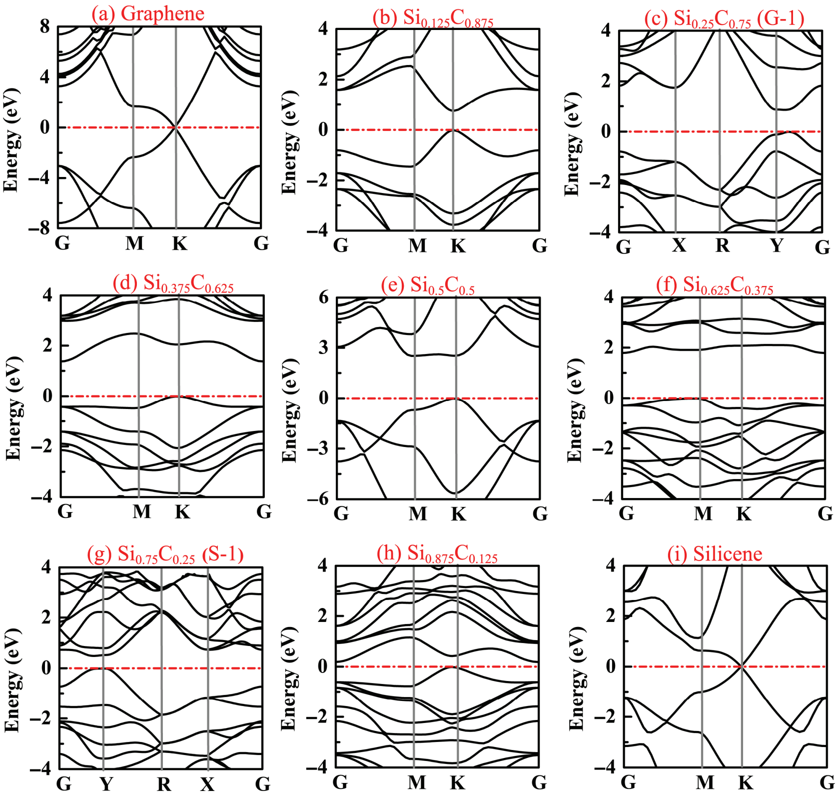

Figure 5 (Color online) Band structures of (a) graphene; (b) $Si_{0.125}C_{0.875}$; (c) $Si_{0.25}C_{0.75}$(G-1); (d) $Si_{0.375}C_{0.625}$; (e) $Si_{0.5}C_{0.5}$; (f) $Si_{0.625}C_{0.375}$; (g) $Si_{0.75}C_{0.25}$ (S-1); (h) $Si_{0.875}C_{0.125}$; and (i) silicene. The horizontal dashed line denotes the Fermi level.

The 2D Si_xC_{1-x} hybrids show diverse electronic properties ranging from semimetals to large-gap semiconductors, and from direct band gap to indirect gap materials, which greatly enriches the electronic diversity of 2D materials. Due to their semimetallic features, graphene and silicene are not suitable for the applications in optoelectronic devices, especially in photovoltaics. Therefore, considerable band gaps opened in Si-C hybrids are precious, extending the potential of graphene-like 2D materials for future applications.

We summarize the trend in the band gaps of 2D Si_xC_{1-x} in Figure 2(c). The changes in the electronic structure are believed to be resulted from interatomic charge transfer effectively tuned by the composition of Si-C hybrids. To gain insights into their electronic origin, the bader charge analysis [30,31] for these structures are performed. The calculated bader charges on the Si and C atom in the 2D sheets are shown in Figure 2(d). Compared with silicon, the carbon atoms tend to gain electrons because of its larger electronegativity. For small Si fraction x, the average electrons on each carbon atom increase from 4*e* to 6*e* with respect to the silicon fraction, because carbon atoms are the majority species and tend to receive electrons from silicon atoms. The bader charges on carbons reach the peak value of 6.54*e* at x=0.5, where each carbon is surrounded by three silicon atoms. After that, the charge value on carbon slightly decreases to 6.1*e* at Si-rich limit. The total bader charge transfer in the unit cells of 2D $Si_{0.25}C_{0.75}$ (G-2) and $Si_{0.75}C_{0.25}$ (S-2) are 4.7 and 4.6 electrons, respectively. In other words, about 2.4 and 0.8 electrons per each silicon atom are transferred to C atoms in 2D $Si_{0.25}C_{0.75}$ and $Si_{0.75}C_{0.25}$, respectively.

We highlight the peculiar electronic structure of $Si_{0.25}C_{0.75}$ (G-2) and $Si_{0.75}C_{0.25}$ (S-2) shown in Figure 6. Similar to graphene and silicene with intriguing electronic properties, the π and π* bands of $Si_{0.25}C_{0.75}$ (G-2) and $Si_{0.75}C_{0.25}$ (S-2) also cross at K point, which can support massless Dirac fermions. Thus, $Si_{0.25}C_{0.75}$ (G-2) and $Si_{0.75}C_{0.25}$ (S-2) are also zero band gap semimetals. The bands for $Si_{0.25}C_{0.75}$ (G-2) and $Si_{0.75}C_{0.25}$ (S-2) are similar except that the top of valence band of $Si_{0.25}C_{0.75}$ (G-2) touches Fermi level at Gamma point. By fitting the π and π* bands at $k=K+q$, the Fermi velocities (V_F) are estimated to be 0.6×10^6 m/s and 0.5×10^6 m/s for $Si_{0.25}C_{0.75}$ (G-2) and $Si_{0.75}C_{0.25}$ (S-2), respectively, which are about half the V_F value reported for graphene (1×10^6 m/s) and very similar to the value of silicene (0.5×10^6 m/s). For a detailed comparison, some important parameters for $Si_{0.25}C_{0.75}$ (G-2) and $Si_{0.75}C_{0.25}$ (S-2) are listed in Table 1.

The thermodynamic stability of 2D $Si_{0.25}C_{0.75}$ and $Si_{0.75}C_{0.25}$ is confirmed via phonon dispersion calculations. The calculated phonon dispersion spectrum of 2D $Si_{0.25}C_{0.75}$ (G-2) and $Si_{0.75}C_{0.25}$ (S-2) is shown in Figure 7. No imaginary

Table 1 Calculated structural parameters of 2D $Si_{0.25}C_{0.75}$ (G-2) and $Si_{0.75}C_{0.25}$ (S-2). Here a (Å), $d_{C\text{-}C}$ (Å), $d_{C\text{-}Si}$ (Å), $d_{Si\text{-}Si}$ (Å), E_{coh} (eV), ΔQ (e), Δq (e), E_G (eV), V_F ($\times 10^6$m/s) represent lattice constant, C—C bond length, C—Si bond length, Si—Si bond length, cohesive energy per atom, total charge transfer in the unit cell, charge transfer per Si atom (ΔQ divided by the number of silicon atoms), energy gaps, carrier Fermi velocities, respectively. Bonding types between Si and C atoms are also shown. For comparison, corresponding values for graphene, silicene, and $Si_{0.5}C_{0.5}$ are also given

Structure	Graphene	$Si_{0.25}C_{0.75}$	$Si_{0.5}C_{0.5}$	$Si_{0.75}C_{0.25}$	Silicene
a (Å)	4.93	5.64	6.20	7.03	7.74
$d_{C\text{-}C}$ (Å)	1.425	1.44	–	–	–
$d_{C\text{-}Si}$ (Å)	–	1.81	1.79	1.81	–
$d_{Si\text{-}Si}$ (Å)	–	–	–	2.25	2.28
E_{coh} (eV)	7.97	6.70	5.99	4.81	3.95
ΔQ (e)	–	4.7	10.1	4.6	–
Δq (e) per Si	–	2.4	2.5	0.8	–
E_G (eV)	0	0	2.5	0	0
V_F ($\times 10^6$m/s)	1.0	0.6	–	0.5	0.5
Bonding type	sp^2	sp^2	sp^2	sp^2	sp^2 /sp^3

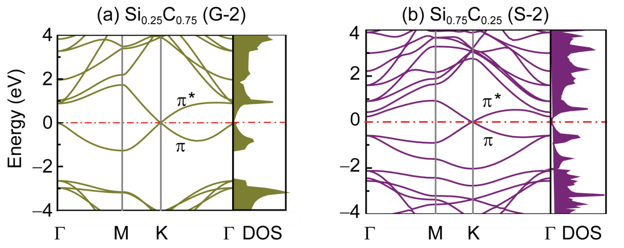

Figure 6 (Color online) Band structure and total density of states (DOS) of (a) $Si_{0.25}C_{0.75}$ (G-2) and (b) $Si_{0.75}C_{0.25}$ (S-2). The horizontal dashed red lines denote the Fermi level. The π and π^* bands crossing at K point are also labeled.

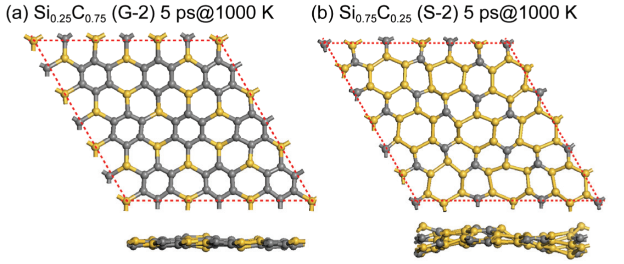

Figure 8 (Color online) Top and side view of snapshots of (a) 2D $Si_{0.25}C_{0.75}$ (G-2) and (b) $Si_{0.75}C_{0.25}$ (S-2) monolayers after 5 ps of *ab initio* molecular dynamics simulation.

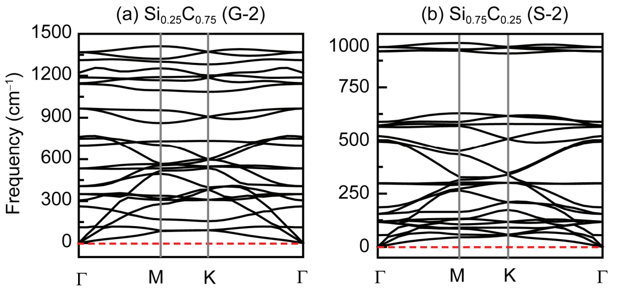

Figure 7 (Color online) Calculated phonon dispersion spectrum of (a) $Si_{0.25}C_{0.75}$; (b) $Si_{0.25}C_{0.75}$.

frequencies are found. The highest frequencies are about 1420 cm^{-1} for $Si_{0.25}C_{0.75}$ and 960 cm^{-1} for $Si_{0.75}C_{0.25}$ in the two phonon dispersion plots. In $Si_{0.25}C_{0.75}$, there is no Si—Si bond while there is no C—C bond in $Si_{0.75}C_{0.25}$. In addition, silicon atom is heavier than carbon atom, which results in the difference in the highest frequencies.

We also perform MD simulations at 1000 K and 2000 K for $Si_{0.25}C_{0.75}$ (G-2) and $Si_{0.75}C_{0.25}$ (S-2) sheets. In these calculations the (3×3) supercells are used to lift the constraint of small unit cells. At 1000 K, the geometries of the two structures are well kept (Figure 8). At 2000 K, the honeycomb structure of $Si_{0.25}C_{0.75}$ (G-2) maintains its structural integrity, with only a small number of atoms deviating from their original positions without destroying any bonds. However, $Si_{0.75}C_{0.25}$ (S-2) turns to be a distorted structure with large disorder at 2000 K during MD simulations. The 2D honeycomb structure has been destroyed after 1 ps simulation and some bonds are broken. We also perform structure optimizations starting from the distorted structures from MD simulations. After full atomic relaxation, the distorted structures for both $Si_{0.25}C_{0.75}$ (G-2) and $Si_{0.75}C_{0.25}$ (S-2) easily recover the planar 2D sheet structure, which confirms their thermal stability.

It has been reported that 2D SiC_2 silagraphene (pt-SiC_2) with planar tretacoordinate building block is metallic due to several bands across the Fermi level from first principles calculations [32,33]. A novel SiC_2 silagraphene (g-SiC_2) [33] with a direct band gap of 1.09 eV in a perfect planar geometry is also predicted, where Si and C atoms adopt sp^2 hybridization and C atoms form delocalized 4 C-domains which are periodically separated by Si atoms. Such a planar 2D structure can be applied to fabricate excitonic solar cells, whose power conversion efficiency critically depends on the interface alignment between the donor and acceptor materials. It is natural to consider the optical properties of the silicon-carbon hybrids predicted here and their potential in photovoltaic applications.

Graphene exhibit zero band gaps, making it unsuitable for controllable transistor operations, consequently limiting

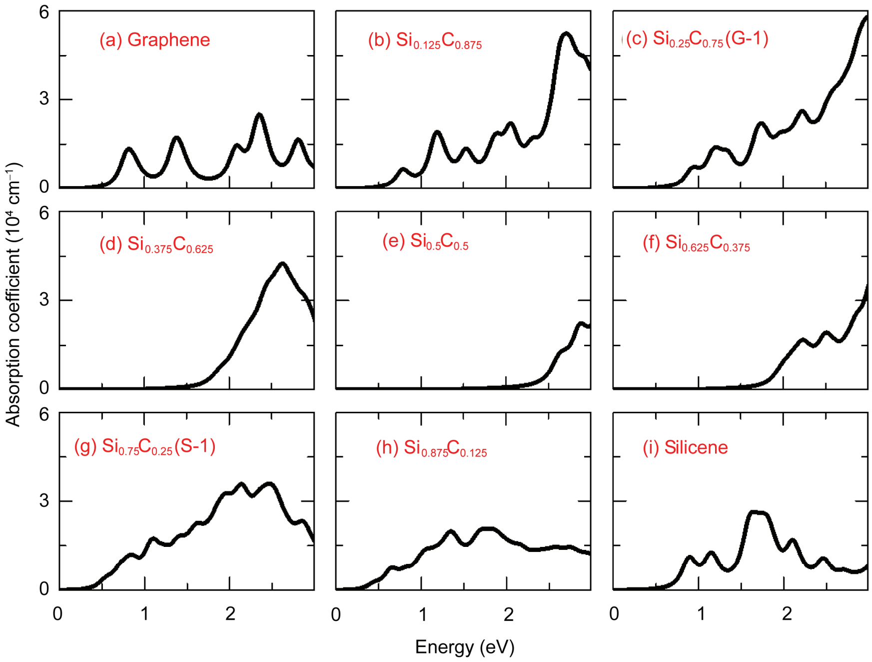

Figure 9 (Color online) Calculated optical coefficients of (a) Graphene; (b) $Si_{0.125}C_{0.875}$; (c) $Si_{0.25}C_{0.75}$ (G-1); (d) $Si_{0.375}C_{0.625}$; (e) $Si_{0.5}C_{0.5}$; (f) $Si_{0.625}C_{0.375}$; (g) $Si_{0.75}C_{0.25}$ (S-1); (h) $Si_{0.875}C_{0.125}$; and (i) silicene, as a function of photon energy.

its widespread applications in optoelectronic devices such as light-emitting diodes and solar cells. Thus, it is necessary to investigate the optical properties of 2D Si_xC_{1-x}. Absorption spectra of the serial of 2D Si_xC_{1-x} structures are plotted in Figure 9. The results show that as we increase the Si concentration, the intensity and position of the main absorption peaks exhibit rather large optical absorption strength. We focus on optical adsorption in the visible light range of 1.5–3 eV, which is of key importance for highly efficient photovoltaic devices. We find the absorption coefficients of Si-C hybrids shown in Figures 9(b), (c) and (g), (h) are higher than those in graphene and silicene. In particular, the $Si_{0.25}C_{0.75}$ (G-1) and $Si_{0.75}C_{0.25}$ (S-1) structures have outstanding strong light absorption in the whole range of infrared and visible region. For $Si_{0.5}C_{0.5}$ with a relatively large band gap, optical absorption in the range of visible light is little and this can be explained by large charge transfer and high ionization potential of the Si and C atoms in this structure. Different absorption properties for different Si/C ratios provide rich choices in the use of 2D group-IV binary materials, so that they can be used in a variety of photovoltaic devices such as excitonic solar cells and photo-detector devices.

4 Conclusion

In summary, we have investigated the trends in the structural and electronic properties of graphene-like Si—C hybrids with different silicon ratios and configurations. The results indicate that, the electronic and optical properties of this new family of silicon-carbon hybrids can be tuned effectively by changing chemical compositions and atomic structures. $Si_{0.25}C_{0.75}$ (G-2) and $Si_{0.75}C_{0.25}$ (S-2) with a honeycomb superstructure remains stable in a planar honeycomb lattice. The 2D Si_xC_{1-x} have tunable band gaps varying from zero to a rather large value (2.5 eV), suggesting versatile electronic properties can be achieved. Optical analysis of 2D Si_xC_{1-x} hybrids indicates that the structures with different Si fractions and configurations can exhibit quite different optical coefficients and some have strong optical absorption in the range of visible light. We expect that the 2D Si_xC_{1-x} sheets predicted here will inspire future experimental and theoretical studies on such 2D materials, and they will come out in laboratory soon to have these interesting properties confirmed.

This work was supported by Ministry of Science and Technology (Grant No. 2012CB921403), the National Natural Science Foundation of China (Grant Nos. 11304176 and 11334011), and "Strategic Priority Research Program B" of the Chinese Academy of Sciences (Grant No. XDB07030100).

1 Novoselov K S A, Geim A K, Morozov S V, et al. Two-dimensional gas of massless Dirac fermions in graphene. Nature, 2005, 438: 197–200

2 Geim A K. Graphene: Status and prospects. Science, 2009, 324: 1529–1534

3 Zhang Y, Tan Y W, Stormer H L, et al. Experimental observation of the quantum Hall effect and Berry's phase in graphene. Nature, 2005, 438: 201–204

4 Wang Z F, Liu Z, Liu F. Quantum anomalous Hall effect in 2D organic topological insulators. Phys Rev Lett, 2013, 110: 196801

5 Cahangirov S, Topsakal M, Aktürk E, et al. Two- and one-dimensional honeycomb structures of silicon and germanium. Phys Rev Lett, 2009, 102: 236804

6 Liu C C, Feng W, Yao Y. Quantum spin Hall effect in silicene and two-dimensional germanium. Phys Rev Lett, 2011, 107: 076802

7 Feng B, Ding Z, Meng S, et al. Evidence of silicene in honeycomb structures of silicon on Ag (111). Nano Lett, 2012, 12: 3507–3511

8 Vogt P, De Padova P, Quaresima C, et al. Silicene: Compelling experimental evidence for graphenelike two-dimensional silicon. Phys Rev Lett, 2012, 108: 155501

9 Fleurence A, Friedlein R, Ozaki T, et al. Experimental evidence for epitaxial silicene on diboride thin films. Phys Rev Lett, 2012, 108: 245501

10 Lalmi B, Oughaddou H, Enriquez H, et al. Epitaxial growth of a silicene sheet. Appl Phys Lett, 2010, 97: 223009

11 Lin C L, Arafune R, Kawahara K, et al. Substrate-induced symmetry breaking in silicene. Phys Rev Lett, 2013, 110: 076801

12 Chen L, Liu C C, Feng B, et al. Evidence for Dirac fermions in a honeycomb lattice based on silicon. Phys Rev Lett, 2012, 109: 056804

13 Bekaroglu E, Topsakal M, Cahangirov S, et al. First-principles study of defects and adatoms in silicon carbide honeycomb structures. Phys Rev B, 2010, 81: 075433

14 Drissi L B, Saidi E H, Bousmina M, et al. DFT investigations of the hydrogenation effect on silicene/graphene hybrids. J Phys Condens Matter, 2012, 24: 485502

15 Dai J, Zhao Y, Wu X, et al. Exploration of structures of two-dimensional boron–silicon compounds with sp^2 silicon. J Phys Chem Lett, 2013, 4: 561–567

16 Luo X, Yang J, Liu H, et al. Predicting two-dimensional boron–carbon compounds by the global optimization method. J Am Chem Soc, 2011, 133: 16275–16280

17 Zhang Z, Liu X, Yakobson B I, et al. Two-dimensional tetragonal TiC monolayer sheet and nanoribbons. J Am Chem Soc, 2012, 134: 19326–19328

18 Wang Q H, Kalantar-Zadeh K, Kis A, et al. Electronics and optoelectronics of two-dimensional transition metal dichalcogenides. Nat Nanotech, 2012, 7: 699–712

19 Mak K F, Lee C, Hone J, et al. Atomically thin MoS_2: A new direct-gap semiconductor. Phys Rev Lett, 2010, 105: 136805

20 Bernardi M, Palummo M, Grossman J C. Extraordinary sunlight absorption and one nanometer thick photovoltaics using two-dimensional monolayer materials. Nano Lett, 2013, 13: 3664–3670

21 Zhong P, Que W X, Zhang J, et al. Enhancing the performance of poly(3-hexylthiophene)/ZnO nanorod arrays based hybrid solar cells through incorporation of a third component. Sci China-Phys Mech Astron, 2014, 57: 1289–1298

22 Wu B, Li W B, Yu H M, et al. Photoinduced charge injection in the metal/organic interface studied by transient photovoltage measurements with bias. Sci China-Phys Mech Astron, 2013, 56: 2012–2015

23 Qin D S, Li G F, Quan W, et al. The improved performance in the ternary bulk heterojunction solar cells. Sci China-Phys Mech Astron, 2013, 56: 530–534

24 Wu W, Wang L, Li Y, et al. Piezoelectricity of single-atomic-layer MoS_2 for energy conversion and piezotronic. Nature, 2014, 514: 470–474

25 Kresse G, Furthmüller J. Efficient iterative schemes for *ab initio* total-energy calculations using a plane-wave basis set. Phys Rev B, 1996, 54: 11169

26 Kresse G, Joubert D. From ultrasoft pseudopotentials to the projector augmented-wave method. Phys Rev B, 1999, 59: 1758

27 Perdew J P, Burke K, Ernzerhof M. Generalized gradient approximation made simple. Phys Rev Lett, 1996, 77: 3865

28 Wang Y, Lü J, Zhu L, et al. Crystal structure prediction via particle-swarm optimization. Phys Rev B, 2010, 82: 094116

29 Togo A, Oba F, Tanaka I. First-principles calculations of the ferroelastic transition between rutile-type and $CaCl_2$-type SiO_2 at high pressures. Phys Rev B, 2008, 78: 134106

30 Sanville E, Kenny S D, Smith R, et al. Improved grid-based algorithm for Bader charge allocation. J Comput Chem, 2007, 27: 899–908

31 Tang W, Sanville E, Henkelman G. A grid-based Bader analysis algorithm without lattice bias. J Phys Condens Matter, 2009, 21: 084204

32 Li Y, Li F, Zhou Z, et al. SiC_2 silagraphene and its one-dimensional derivatives: Where planar tetracoordinate silicon happens. J Am Chem Soc, 2010, 133: 900–908

33 Zhou L J, Zhang Y F, Wu L M. SiC_2 siligraphene and nanotubes: Novel donor materials in excitonic solar cells. Nano Lett, 2013, 13: 5431–5436